

# All-optical intraocular sensor implant for on-demand assessment of high-resolution ocular hemodynamics

Draft by Jeong Oen Lee (12/5/2017)  
Limitation :4000 words for JBO Letter

## 1. Introduction

Implantable [ref] or wearable biosensors [ref] are able to produce exquisitely detailed physiological data from patients. The direct and on-demand monitoring of health-related physiological parameter can open up vast opportunities for disease prevention, health promotion, as well as earlier disease detection.

In ophthalmic applications, accurate, continuous, and on-demand assessment of ocular hemodynamics has been emphasized in the pathology point of view [ref]. The need for careful and frequent monitoring of ophthalmic parameters have taken increased interest in the development of implantable or wearable ocular sensors [ref]. As an organ, the eye requires constant perfusion during dynamic changes in blood pressure. It is logically understood that insufficient blood flow to any organ is a contributory factor in disease processes. A recent report suggests that ocular ischemia may trigger glutamate-mediated toxicity, attenuate ganglion cell function and contribute to retinal nerve fiber loss [ref. Osborne et al. 1999, Andrzej et al. 2011]. Moreover, increasing evidence suggests that vascular abnormality and altered hemodynamics in ocular system play important roles in the progression of open angle glaucoma (OAG) [ref] and the development of diabetic retinopathy [ref]. Likewise, our understanding of the correlation between the ocular hemodynamics and the severe ophthalmic disease progression is still evolving as the advancement of sensing and imaging techniques provide high-quality physiological information.

Ocular pulse amplitude (OPA) is one of important parameters representing the ocular hemodynamics. In accordance with the cardiac cycle, the pulsatile filling of the choroid with blood via the short ciliary arteries generates the oscillations of the blood flow into the eye [ref. Thiel 1928; Bynke & Schele 1967; Perkins 1981; Schmidt et al. 2001]. Typically, the intraocular pressure (IOP) increases by 2–3 mmHg during the systolic phase in a cardiac cycle compared to the diastolic phase (Kaufmann et al. 2006). This pressure difference is represented by the OPA in a periodic profile of the ocular pulsation.

The OPA assessment and primitive studies on ocular hemodynamics have been performed by Pascal Dynamic Contour Tonometer (DCT). The DCT is a relatively simple device, thus is the most popular technique for the ocular hemodynamics assay so far.<sup>1</sup> Combined with other clinical or laboratory data, OPA alterations may give clues to the possibility of adverse effects from any hemodynamic compromise of the eye [ref]. Some studies suggested that patients with glaucoma or diabetic retinopathy may present the different OPA profile compared to normal subjects [ref]. Accurate OPA assessment can be also used for carotid artery stenosis diagnosis [ref]. Nonetheless, the measurement stability and reliability needs to be further explored. For the DCT examinations, a physical contact between the corneal surface and a tonometer tip is important to obtain reliable estimation of the OPA while minimizing influences of the corneal properties. For example, the tonometer tip has to be positioned on the patient's cornea for at least 4–5 s during the measurement. [ref] If the patient

is not able to prevent eye movements during that time, IOP measurement is disturbed, resulting in lower reading quality. Also, the damping induced by physical contact between corneal surface and the probing tip degrades the mechanical responsiveness, and thus might hinder to visualize the occurrence of systolic and diastolic phases in a singular ocular pulse.

This resolution limitation in DCT technique was conquered by imaging systems. High-resolution ocular hemodynamic profile can be depicted by measuring ocular blood flow or velocity, which are another possible parameters being used for ocular hemodynamic analysis.<sup>2</sup> Color Doppler imaging (CDI) is by far the most commonly utilized and established methodology to measure aspects of ocular circulation in clinical practices. CDI is able to accurately visualize retrobulbar blood vessels, such as the ophthalmic, central retinal and can image temporal short posterior ciliary arteries as well as measure peak systolic blood flow (PSV) and end diastolic blood flow (EDV) velocities. Other approaches, such as Laser Doppler flowmeter (LDF), the retina vessel analyzer (RVA), Fourier-domain (FD) OCT, are also currently in use and measure different aspects of ocular blood flow. Aforementioned techniques, however, require highly skilled, experienced technicians and can be expensive. Further, the availability of imaging technologies is greatly limited.<sup>3</sup>

To facilitate frequent and on-demand monitoring of ocular hemodynamics, implantable or wearable sensors are a promising approach [ref] pushing through the availability limitations in aforementioned ophthalmic instruments and imaging technologies. However, performance of the current sensor technology [ref] was not yet able to offer superior sensitivity and sufficient temporal resolution compared with the CDI technique; with remarkable sensing resolution, the CDI technique determines essential ocular hemodynamic parameters, such as PSV, EDV, RI, extracted from systolic and diastolic pattern analysis. It is important to note that the hemodynamic phase classification is a key step towards understanding the dynamic ocular perfusion associated with ocular blood flow, whereas the profiling resolution of current ocular sensors is not sufficient to perceive systolic and diastolic phases [ref]. If it is possible to continuously record high-resolution ocular perfusion pattern *via* an implantable or wearable sensor framework, leading us to retrieve hemodynamic factors with respect to chronic ocular disease progression for long-term perspective, it will be beneficial in suggesting new ophthalmic pathologies, earlier disease detection, and better treatment options. Although extensive studies have been conducted in many implantable and wearable sensors, none of the reported methods offer an accurate, easy-to-use ocular monitoring technology for routine recording of high-resolution ocular perfusion.

## 2. Materials and Methods

### 2.1 System Overview

To address these issues, we propose an all-optical ocular pulsation profiling technique by combining an implantable optomechanical sensor (**Fig. 1a**) and an easy-to-use handheld detector (**Fig. 1b**) that enables on-demand assessment of high-resolution ocular hemodynamics. Our remote optical assessment approach that analyzes the dynamic fluctuation of reflected spectrum generated by a tungsten light bulb illumination allows us to obtain intact and high-resolution ocular pulsation profile without making any physical contact on cornea or demanding sophisticated imaging techniques. Moreover, the long-lasting sensor implant and the

compact portable detector enhances the system availability in laboratories, clinics and possibly home environments.

An implantable IOP sensor has been developed for many years associated with ophthalmic researches, thereby the sensor fabrication, characterization, surgical procedure, materials, and immunoassays are well established. Particularly for patients who already had to use ocular devices and implants, it is an intriguing approach to accumulate an additional functionality of making the high-resolution ocular hemodynamics assessment on the existing ocular sensor framework, allowing the patients to be benefited from matured clinical protocols, reliability of the system, and potentially parallel monitoring of multiple physiological parameters. In our previous works, we established a sensor implant for static IOP monitoring using a Fabry-Perot optomechanical cavity. We also improved its bio-compatibility and readout reliability with various material-based strategies [ref, ref] and mapping algorithm improvement [ref].

In this work, we present a technique to greatly improve temporal and sensing resolution of the optical sensing system as well as its adaptability. As a result of the resolution advance, it is possible to track the dynamic fluctuation of the ocular pulsation profile, and it even visualizes systolic and diastolic phases in a continuous ocular assessment with a simple remote detecting platform. This ocular hemodynamic phase classification has been of interests to many ophthalmologists who want to understand the hemodynamics factors with respect to the ocular disease associations and progression. Moreover, with the pulse waveform analysis, vascular parameters can be displayed together with IOP and OPA, which essentially achieves multi-physiological parameter monitoring system. The phase classification was challenging in previous DCT techniques and other conventional IOP sensors built by microwave modalities.

In medical aspects, our system presents several key features. **First**, for the dramatic improvement of the dynamic sensing resolution, we report a direct intensity analysis (DIA) method that significantly improves the sensitivity of the optical acquisition system to perceive the subtle pressure fluctuation produced by ocular perfusion. The DIA method directly detects intensity variation in the reflection spectra of an optomechanical device driven by ocular perfusion. Our previous resonance-shift detection [ref] method provides only 5 levels of the pressure identification resolution in principle, whereas the DIA method provides 10-fold higher sensitivity in the pressure identification resolution for the unit pressure change ( $<1\text{mmHg}$ ). **Second**, we simplify and elaborate the remote optical detecting system in a single-hand portable size and reduced weight comparable to smartphone device to enhance the clinical usability and enable the routine recording of high-resolution ocular perfusion. For the sensor interrogation, the detecting device uses a clinically safe white-light source and the working distance is over 3 cm. **Third**, our approach enables parallel monitoring of multi physiological parameters, such as IOP, OPA, vascular index, through the unitary optical spectra acquisition. Using our previous method, the IOP and OPA baseline can be obtained with the accuracy of 0.01 mmHg from spectra-to-pressure mapping algorithm associated with cavity resonance shift and advanced mapping algorithms. Additional vascular parameters are quantified with the DIA method. We verified this capability by comparing the optical signal obtained by DIA system and the reference measurement from cardiovascular monitoring system including ECG and PPG (Fig. 1c and 1d).

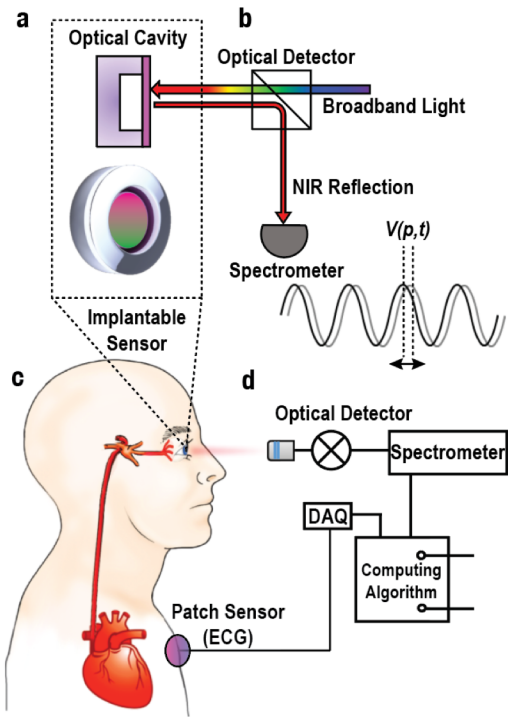


**Fig.1** *In-vivo* ocular pulsation monitoring system. (a) Schematic of an implantable optomechanical cavity sensor (top) and a tilted 3-d illustration of the sensor (bottom). (b) Simplified diagram of the remote optical detector. (c, d) A testing subject with the integrated detecting system.

## 2.2 All-Optical Sensing Platform: Sensor and Detector

The main components of our system are an implantable optomechanical cavity device (Fig. 2a) and a hand-held remote optical detector recording the reflection spectra (Fig. 2b). The optomechanical cavity device comprises a flexible and transparent membrane placed above a micromachined silicon mirror surface. The cavity's resonance shifts caused by the membrane deformation with respect to ambient pressure change can be detected by broadband light illumination and the reflection measurement.

Since we suggested the simplest detection scheme capable of being made with a few ordinary optical components, it was possible to transform our previous detection systems [refs] into a substantially miniaturized form. Design of a compact handheld detector is inspired by a monocular ophthalmoscopy [ref], but it incorporates with dichroic mirrors, an objective lens, and a clinically approved light source with broadband optical spectrum (500 – 1000 nm) that is powered by common batteries (Duracell MN2400 AAA 1.5V, Duracell Inc., Connecticut, USA). As small optic components are integrated in a plastic housing, the portable detector is lightweight (159 g) comparable to mobile phone. The manipulation of the portable detector is very simple, almost identical to magnifying lens that are commonly available in clinics. Thus, an examiner can easily find and follow the location of the implanted sensor through either an attached USB camera (STC-MB133USB, Sentech Co., Atsugi, Japan) or an eyepiece (Fig. 2c and 2d). In the optical detector, the illumination optical path is coaxially built with the detection optical path that an examiner can notify the correct optical alignment by observing the brightest reflection occurring upon the sensor image. When the detector's

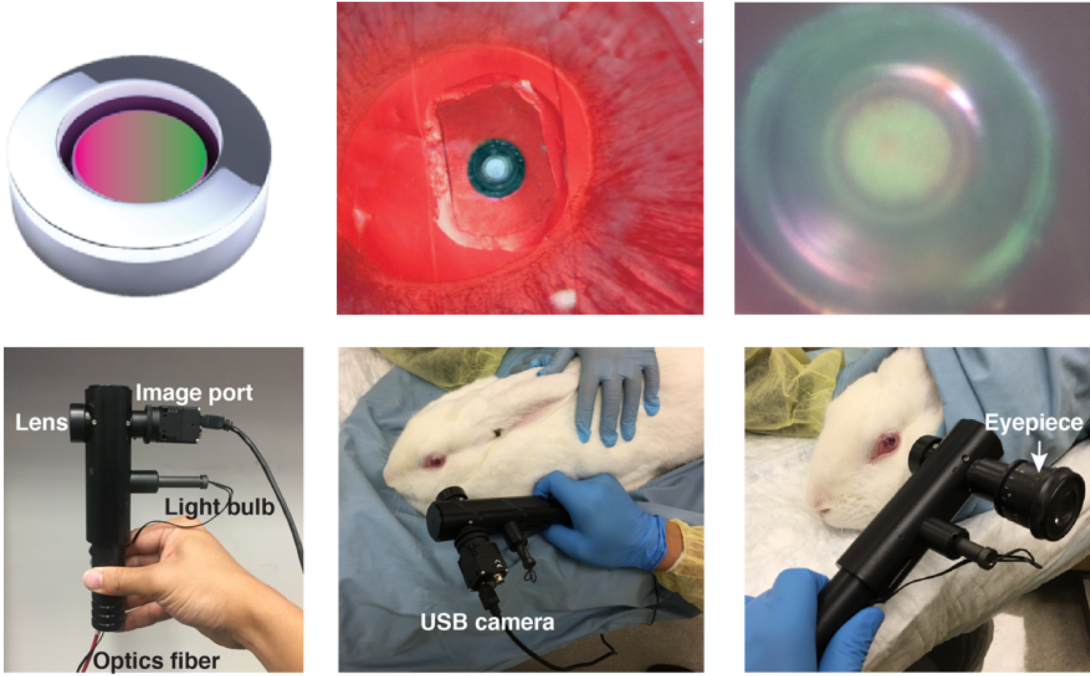


**Fig.2 All optical ocular assessment system.** (a) Implantable optomechanical sensor (b) Handheld optical detector

illumination is perpendicularly aligned to the sensor surface that valid optical spectra with discernable peaks and valleys are identified by spectrum recognition algorithm, our software automatically initiates the data recording and performs the post computation process with the recorded spectra. The data processing basically includes the static IOP identification step using a traditional cavity resonance tracking method [ref], and the advanced dynamic intensity analysis (DIA) that retrieves ocular pulsation contribution in high-resolution profile. The implemented algorithms and automated software are packaged in graphical user interface (GUI) so that our system minimizes the examiners' efforts in the measurements, enhancing the adaptability in various testing environment without extensive user training.

### 2.3 In-vivo Data Acquisition System

In order to verify the high-resolution profiling ability and performance of our ocular pulsation monitoring system, we carried out *in-vivo* data acquisition experiments on awoken animals. Prior to the sensor implantation into testing animals, all sensors should be pre-tested on a bench setup, and then characteristic curves with device parameters were extracted. Sterilization was performed by placing the devices into 70% ethyl alcohol for 24 hours before the surgical implantation. Next, the optomechanical sensors mounted on delivery silicone strips ( $2 \text{ mm} \times 10 \text{ mm} \times 0.1 \text{ mm}$ ) were implanted inside eyes of New Zealand white rabbits following the surgical protocol similar to our previous work [ref].

The handheld optical detector perceives the ocular pulsation profile represented as subtle cavity resonance perturbation in the reflection spectrum measurement. Since the optomechanical sensor is located right below the corneal surface where the light transmission is naturally high (transmission  $\sim 95\%$ ), the incoherent

and clinically safe light source, such as a mini light bulb, is adaptable for our system. We selected an incandescent light bulb with tungsten filament ([model here](#)) as an illumination source that provides a uniform and wide range spectrum across the wavelength between 500 to 1000 nm following the characteristics of blackbody radiation [ref]. Coupled with this light source, the signal-to-noise (SNR) ratio of the reflected cavity resonance is designed to have the maximum at around 800 nm. As such, we used a VIS-NIR spectrometer (MAYA 2000 Pro, Ocean Optics, Dunedin, FL, USA) with wavelength range of 780–1200 nm, spectral resolution of 0.22 nm, to obtain an excellent NIR sensitivity in the wavelength region of interest.

For the high temporal resolution, the spectra sampling frequency was set to 100 Hz to seamlessly track the ocular hemodynamics occurring around 1-5 Hz. Also with the same sampling rate, cardiac activities of the testing animal were separately monitored in two different aspects as reference measurements. ECG profile representing electrical signal of the [rabbit heart](#) was recorded by attaching three electrodes on the rabbit chest. And blood pulsation was recorded from the rabbit ear with a PPG method combining a probe device to a commercial digital DAQ board (Arduino Uno, Arduino, Somerville, MA, USA). All voltage outputs from cardiac monitoring devices and the optical spectra measurements are simultaneously restored in a control laptop computer in millisecond time resolution. Each measurement session takes about 30-60 seconds. Thus 3000-6000 optical spectra are processed.

### 3. Results

Our approach for ocular hemodynamic mapping consists of three steps: (1) *in-vivo* optical spectrum measurement; (2) fundamental IOP baseline and OPA retrieval from peak and valley detection; (3) high-resolution pulsation mapping using a direct intensity analysis technique.

#### 3.1 In-vivo Optical Spectrum Measurement

Once the sensors were implanted in rabbit eyes, sensor's cavity resonance can be measured by optical interrogation with broadband light illumination. This optical spectrum is a mainstay of post signal analysis to acquire ocular parameters. After sensor implantation, the very first optical measurement could be done with using both microscope system and the portable detector alternatively (**Fig. 3**). The spectrum comparison in two different systems quantifies the handheld detector's performance. Furthermore, we could confirm by two different detectors that the surgical procedure was well performed without causing any optical or mechanical degradation on the sensor implants.

The initial reference assessment was conducted on an anesthetized rabbit using a microscope detector. All optical components are fixed on a stable 3-axis translational stage (**Fig. 3a**) to minimize mechanical vibration. In this case, the rabbit's respiration is the only vibration source that can cause irregular misalignment of the focal spot with respect to the sensor's active core. Nonetheless, continuous spectra acquisition and following signal processing steps can efficiently filter out irrelevant signals (**Fig. 3b**). The valid spectra are automatically identified by resonance pattern recognition. Since the optomechanical cavities have unique spectral characteristic with multiple cavity resonance dips that cannot be created by tissue or organ, the filter algorithm detects the valid spectra when the cavity resonance presents sufficient peak-to-valley amplitude and designated number of resonance dips (**Fig. 3b**). In addition to this, it was useful to position the detector while monitoring the sensor location with USB camera to maximize the number of valid measurement.

Confirming the *in-vivo* optical measurement using a standard microscope platform, the same technique was applied to hand held detector system. Due to a multi-degree-of-freedom of positioning, the handheld detector is convenient for tracking the sensor implant, and enables us to remotely interrogate an awoken rabbit without anesthesia and subject disturbance (**Fig. 3c**). The collected and filtered spectra from the handheld detector measurement were in good agreement with the microscope measurement. The SNR of the microscope system is 20 dB while the handheld detector presents 18 dB (**Fig. 3d**).

The interrogation stability can be quantified by investigating the accumulated spectra. For this, individual spectrum collected by the spectrometer was instantly accumulated into the computing system for 60 seconds with a sampling rate of 100 Hz, while the optical alignment and measurement upon a testing animal had been in progress. The noise removal process and peak/valley detection process executed in parallel per the individual spectrum acquisition with process time of about 50  $\mu$ s. After the *in-vivo* data acquisition session, the accumulated spectra can be plotted on a color-coded map as shown in **Fig. 3e**. The periodic color pattern with bright and dark color appearance presents the valid cavity resonance in which the high intensity in the spectrum was mapped into bright color. The 20 seconds in the plot with the periodic color pattern indicates that the optical detector was stably 'locked-in' upon the

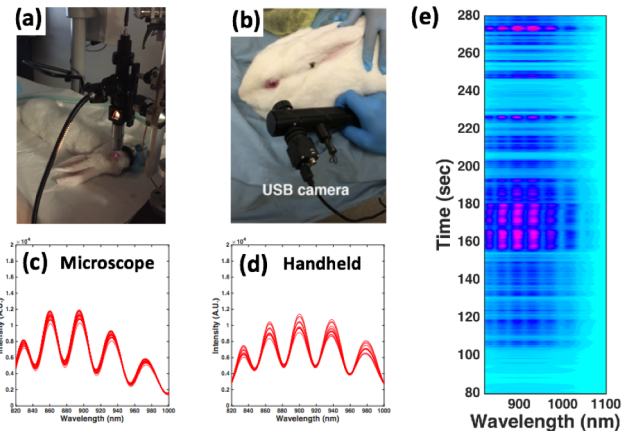


Fig. 3 SNR and stability of *in-vivo* measurement using both optical detectors (microscope & handheld)

sensor's core cavity. The average SNR over the 'locked-in' time was 17.8 dB and number of valid spectra was 1500 among 6000 of the total stored frames. This factor represents the qualification of each measurement session and the large number of valid spectra improves the statistical accuracy.

We found that optical degradation caused by absorption and aberration properties of ocular tissues are ignorable (~90%) as long as the sensor is placed within 1cm diameter of the central optical axis of the rabbit eye. Our handheld detector and the microscope detector that was used in the sensor calibration on bench tests show the identical optical spectrum from the same sensor with SNR of 15-20dB (**Fig. 3c and 3d**).

#### 3.2 IOP baseline and OPA retrieval

IOP and OPA are important ophthalmic parameters that are generally measured by DCT, but it necessarily involves physical contact on a corneal surface. In contrast, our system measures IOP and OPA without demanding any physical contact on the cornea. Our sensor and detector system uses remote optical sensing for determining a fundamental IOP baseline from peak/valley location analysis on the optical spectrum. Then the OPA can be retrieved by analyzing small pressure fluctuation on the IOP baseline.

Measuring a reflection spectrum from an optomechanical sensor, the static ambient pressure, referring IOP, can be instantly back-calculated by traditional cavity resonance shift principle [ref]. In *in-vivo* experiment, such IOP indicates a reference central pressure of the hemodynamically driven perfusion component. However, because the peak/valley locations of all devices could be different at a certain pressure, it is necessary to calibrate devices in a pressurized chamber before the implantation.

We characterized a fabricated sensor in a pressurized chamber with two different mapping algorithms. Particularly, fast mapping speed and the measurement accuracy are key factors in ocular hemodynamic assessment. We exploit a support vector regression scheme to satisfy this requirement. For the performance verification, we implemented the support vector regression approach and compared it to original spectrum-to-pressure mapping algorithm based on optomechanical model (OMM) as shown in **Fig. 4**.

The tests were performed by measuring the pressure response of the optomechanical sensor with the readings from the reference electronic pressure sensor while linearly controlling the pressure from 0 mmHg to 40 mmHg. Typically, when optomechanical sensors with the SNR of 15-20 dB have been incorporated with an original OMM mapping method, it presented the IOP mapping accuracy of  $\pm 1$  mmHg.

utilizing a support vector regression scheme on the mapping algorithm, we reduced the computation error caused by non-ideality between empirical device characteristics and a conventional theoretical model. For example, when compared to the digital pressure gauge, measurements using the conventional IOP mapping method showed considerable fluctuations (**Fig. 4a**): the root-mean-square error (RMSE) and the peak-to-peak fluctuation were 1.96 and  $\pm 8$  mmHg, respectively. In contrast, a machine learning technique based on a Support Vector Machine (SVM) approach exhibited an RMSE of 0.58 mmHg and peak-to-peak variation less than  $\pm 0.1$  mmHg over the entire pressure range (**Fig. 4b**), which indicates an order of magnitude accuracy improvement for the baseline IOP identification.

Another notable feature of the SVM algorithm use is improvement of the computation speed. Per sample evaluation time is only 0.157 milliseconds (ms) for SVM method, whereas the OMM method takes 25 ms (**Fig. 4c**). Such significant time

reduction allows to perform additional signal process, for instance digital de-noising and spectra validation between a given sampling interval (10 ms) resulting in real-time visualization of IOP and OPA with minimum noise factors.

For *in-vivo* verification, we acquired optical spectra from an implanted sensor using a portable detector, and mapped a IOP profile with the suggested SVM method (**Fig. 4d**). For the two consecutive measurements - it took around 12 secs for each, the mean IOP of 16.7 mmHg was measured. In the magnified section (**Fig. 4e** and **4f**), the height of the periodic IOP fluctuation indicates OPA with the amplitude of  $\pm 1$  mmHg and the frequency of 4 - 5 Hz. We carried out concurrent ECG measurement representing the testing animal's heartbeat and verified that the cardiac cycle was matched to the OPA frequency.

### 3.2 High-resolution Ocular Pulsation Profiling

To achieve further improvement of mapping resolution in ocular pulsation profile, we suggest a direct intensity analysis (DIA) technique. As described earlier, a steady state IOP should be retrieved by tracking the wavelength shift of the cavity resonance. As such, it determines a fundamental pressure baseline. In addition

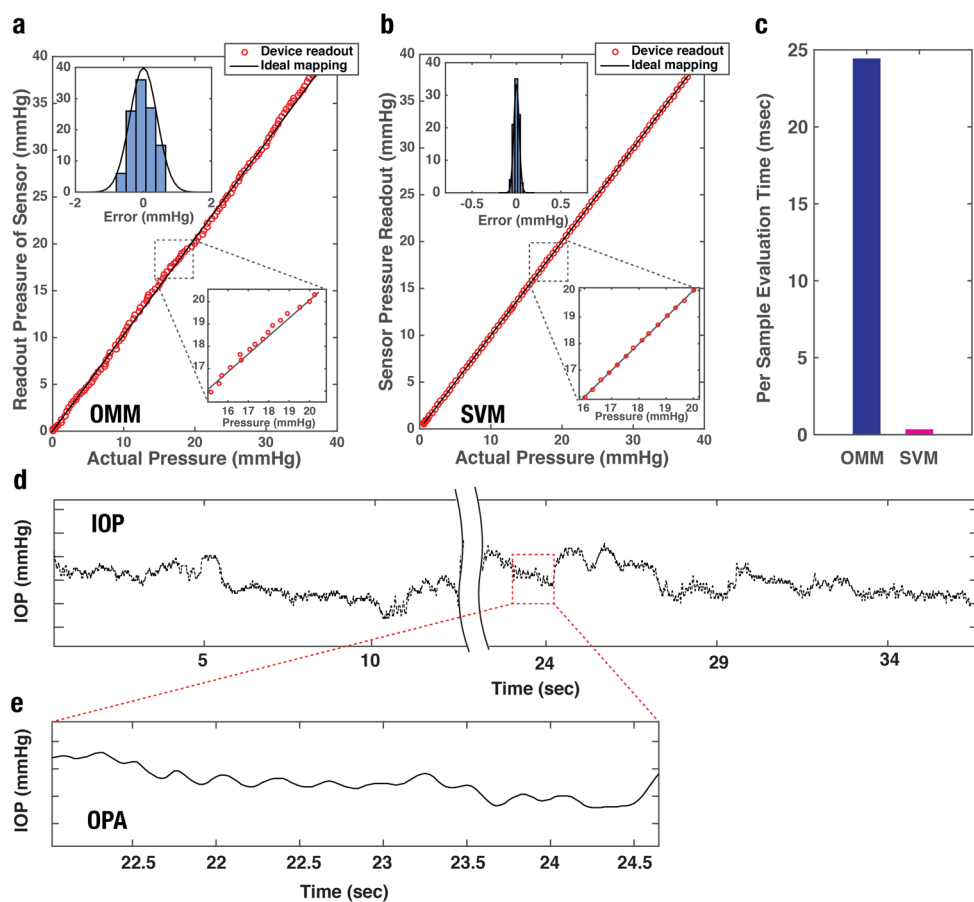


Fig. 4 Sensor readout algorithms using OMM and SVM. *In-vivo* verification of IOP and OPA using the SVM-based mapping method.

to this, the DIA technique measures relative intensity fluctuation that depicts the delicate pulsation components on the IOP baseline.

The DIA technique dramatically enhances probing resolution compared to the wavelength detection. This sensitivity improvement can be understood with a cavity resonance perturbation diagram (**Fig. 5a**) representing the resonance shift property of an optomechanical sensor along the wavelength (x-axis) and intensity (y-axis). Blue and red curves indicate two alternating pressure status driven by ocular perfusion. Essentially, the optical profile of our optomechanical cavity sensor shifts into transvers direction (wavelength axis) as a function of pressure. The maximum pressure difference in the two status, herewith referred to OPA, is about 1-2 mmHg [ref] and this difference corresponds to the wavelength change ( $\Delta\lambda(t)$ ) about 1 nm in the fabricated optomechanical sensor. However, the optical resolution of the detecting system is only 0.2 nm, limited by the size of diffraction grating of a spectrometer. Hence, the peak/valley wavelength detection method provides 5 levels of the pressure identification resolution in principle, then the minimum pressure resolution is 0.2 mmHg.

Whereas, the DIA method provides 10-fold higher sensitivity in the pressure identification resolution. When the reference wavelength is selected between the middle of the cavity resonance (**Fig. 5a**), the intensity difference ( $\Delta I(t)$ ) along the 1 mmHg of pressure change induces the reflection intensity change of 2400–2600 photon counts on the y-axis. Regarding the fact that electronic noise of the spectrometer is only 50 photon counts, the DIA method offers about 50 levels in the pressure identification resolution; this is an order of magnitude higher resolution than the peak/valley wavelength detection method for the given pressure change.

As a result, high-resolution periodic patterns induced by respiration motion and ocular pulsation become distinguishable after exploiting the DIA approach even without any post signal processing on the raw intensity as shown in **Fig. 5b**. Whereas the

peak/valley wavelength detection could not identify the ocular pulsation pattern between the respiration pattern (**Fig. 5c**). As the peak/valley identification method includes linear fitting algorithm, some informative spectra could be eliminated during these approximation process associated with the fitting or filtering steps. For example, two slightly different spectra can be mapped into the same peak/valley values in the peak/valley detection process, even if the same spectrum data was used with the DIA method.

**Figure 5d** shows untreated *in-vivo* intensity data with respect to the measurement time at the reference wavelength of 850 nm. In the profile, the low-frequency saw-tooth-like pattern (0.5–2 Hz) indicates the intensity fluctuation generated by respiration motion. And, the high-frequency intensity fluctuation (~4 Hz) between the respiration pattern was measurement of the ocular pulsation. After removing the low frequency components, passing the raw intensity profile into a digital bandpass filter (pass band: 3–12 Hz), the ocular pulsation profile only remained as shown in **Fig. 5e**. In the zoomed in plot (**Fig. 5f**), systolic and diastolic phase of the ocular pulse are clearly shown. This cardiac phase classification is a mainstay of the

### 3.5 Multi Parameter Profiling

Our system specifies four major parameters associated with ophthalmic pathology. And dynamic parameters, such as DOP, PSV, EDV, RI, are retrieved from the DIA technique.

A single optical measurements are performed by all-optical sensing and the following spectrum analysis, and the physiological parameters are obtained by secondary computation. In the cavity resonance analysis, the IOP and OPA are computed by the peak/valley wavelength detection.

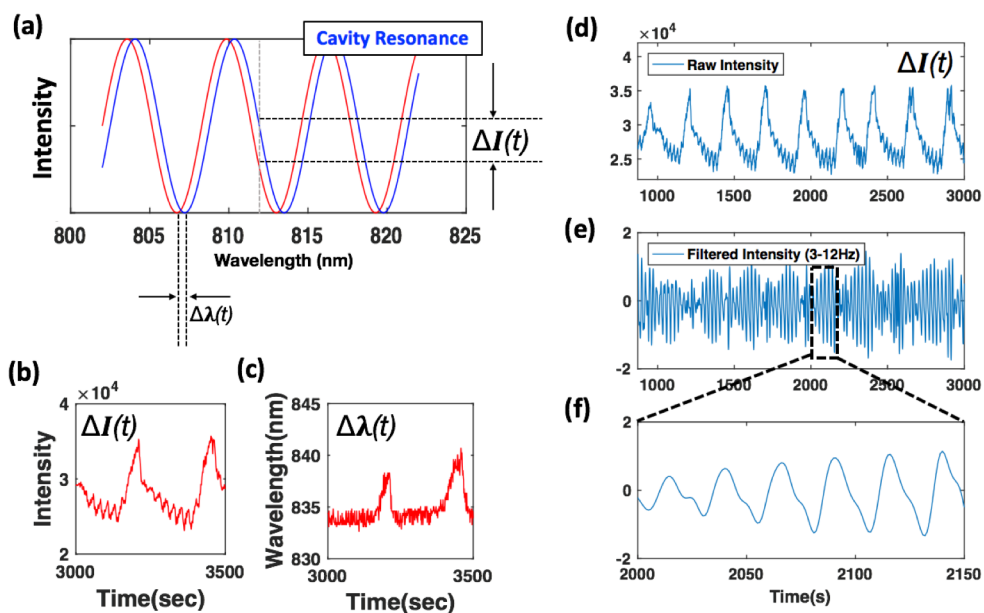
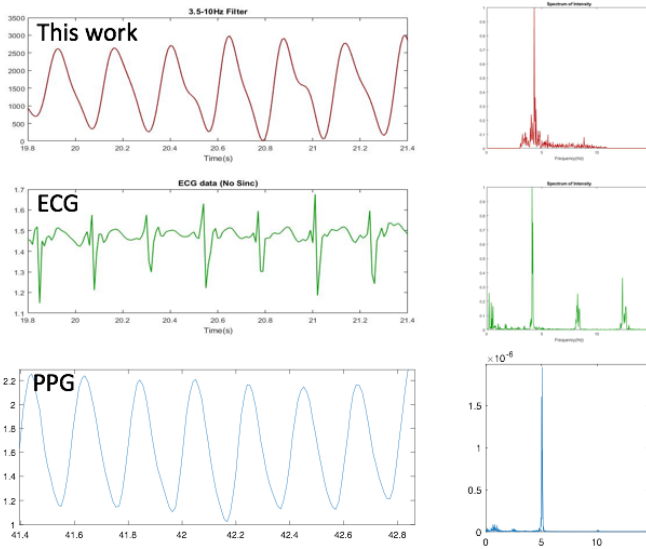


**Fig.5 Ocular pulsation computed from the direct intensity analysis (DIA) method.** (d) Time-dependent intensity fluctuation the probing wavelength of 850 nm. (e) Intensity profile processed by a digital bandpass filter (3-12Hz). (f) Zoomed-in intensity profile for 1.5 second presenting *in-vivo* ocular pulsation profile.



#### 4. Conclusion

An implantable IOP sensor has been developed for many years associated with ophthalmic researches, thereby the sensor fabrication, characterization, surgical procedure, materials, and immunoassays are well established. Therefore, for patients who already had to use ocular sensors, it is an intriguing approach to combine an additional functionality of making the high-resolution ocular hemodynamics assessment upon the existing ocular sensor platform, leading the patients to be benefited from multi parameter monitoring. However, this concept has been rarely demonstrated [ref], despite its clinical utility.

A key objective of the system development approach is to enable high-performance and cost-effective ocular pulsation monitoring by incorporating 1) implantable optomechanical sensor, 2) remote optical detector, 3) ECG and spectral data acquisition system, and 4) post signal processing algorithm. For the visualization of high-resolution *in-vivo* ocular pulsation, achieving high signal-to-noise ratio (SNR) in the spectrum readout is a mainstay. Because hemodynamic activities and fluid flow in an anterior chamber are very subtle by which only a slight amount of reflection spectrum change will be measured, it is important to confirm whether the cavity resonance in *in-vivo* measurements are comparable to the prior bench test that guaranteed sufficient pressure identification resolution of 0.1 mmHg with the SNR of 15dB.

Associating with other examinations, the collected physiological information may suggest different aspects of ocular hemodynamics and the chronic disease progression factors because continuous and long-term acquisition of the high-resolution perfusion profile, hardly found in other technologies, is available on the sensor-based approaches.

## miscellaneous

We implemented the pressure identification algorithm that converts peak/valley features of the reflection spectra into pressure value using software techniques. To achieve a fast and accurate parameter conversion from the detected peak/valley locations to pressure value, various machine learning algorithms including, Artificial Neural Network (ANN), Support Vector Machine (SVM), and Decision Tree Model (DTM) have been used to optimize the identification error and the process time. (will describe more about it)

We have been achieving an optical pressure sensing platform with the pressure resolution of 0.1 mmHg by coupling broadband white-light into a sensitive micro-optomechanical-cavity implant (**Fig. 1a**) and analyzing the spectra of the optical reflection (**Fig. 1b**). Moreover, by optimizing the spectra analyzing algorithm based on various machine learning techniques, the pressure resolution and the computation performance are an order of magnitude enhanced over our previous results that lead us to provide super-resolution pressure sensing (0.01 mmHg) and fast-computation time (100  $\mu$ s/spectrum) capability. This enhanced mapping capability enables to visualize cardiovascular activities, such as systolic and diastolic patterns, reflected on ocular pulse waveforms.

Once the qualified accumulated optical spectra are obtained from an implanted optomechanical sensor, a time-dependent pressure profile can be instantly computed by either physical model [ref] or enhanced mapping algorithm created by machine learning techniques [ref] as shown in **Fig. 4(a)**. Those mapping methods mainly relied on the wavelength detection of peak/valley locations in the resonance spectra by which the ambient pressure can be back-retrieved from the pre-established calibration parameters for each sensor. Particularly, one of our approaches utilized an artificial neural network (ANN) algorithm [ref. IEEE sensors] that used peak/valley locations as training features and provided fast and accurate pressure mapping capability. But it could not visualize discernable ocular pulse patterns as shown in **Fig. 4(b)**.

We optimized the pressure mapping algorithm by using a decision tree model [ref] and provided the pressure accuracy of 0.01 mmHg on a bench test that is an order of magnitude enhanced compared to the previous mapping method. Plus, we applied a wavelet transform technique upon the untreated pressure profile and suppressed irrelevant noise components as shown in **Fig. 4(c)**. As the noise power factor is reduced to **XX** % of the stand-alone mapping technique, combination of the tree model and the wavelet filtering method offered a clear pulsation profile even though the same untreated *in-vivo* data was used as presented in **Fig. 4(a)**. In the zoomed-in plot for 2 seconds (**Fig. 4d**), clear ocular pulsation profile could be verified with the ocular pulse amplitude of **X** mmHg and the pulsation frequency of **Y** Hz after high-frequency background noise and low-frequency respiration pattern (0.5–2 Hz) were removed. The frequency of ocular pulsation calculated by FFT is also in agreement with previous clinical studies [ref] and our concurrent ECG measurement.

Although super-resolution ocular pulse is not demonstrated with the described technique, it would be still useful in a couple aspects. First, since low-power ASIC technology is well established to implement training/mapping functionality of the decision tree model and wavelet-based filters, it will be possible to integrate our post data processing system on a single IC platform in the future. Then, the low-power and compact property of the integrated circuit will promote the further miniaturization of the detecting system. Second, even without the IC integration, our current computing platform is still less inexpensive and compact compare to OCT and DCT, while the accurate and fast visualization capability of the ocular pulsation has been widely demanded in clinical applications including glaucoma, diabetic retinopathy.

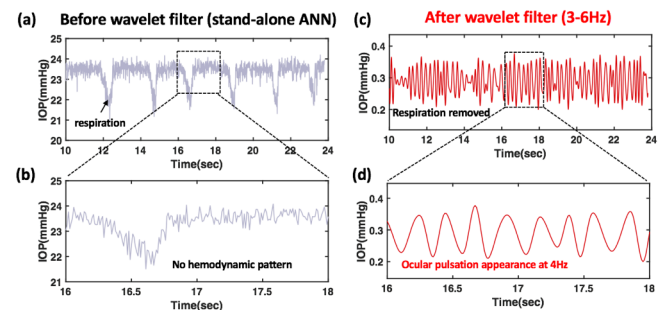


**Fig.4 Ocular pulsation computed from the spectral analysis.** (a) Pressure profile obtained by ANN algorithm. (b) Zoomed-in profile for 2-seconds time. (c) Pressure profile obtained by decision tree model and wavelet filtering technique. (d) Ocular pulsation profile shown in the 2-seconds zoomed-in profile.

## 5. References

1. Katsimpris, J. M.; Petropoulos, I. K.; Pournaras, C. J., Ocular pulse amplitude measurement after retinal detachment surgery. *Klinische Monatsblätter für Augenheilkunde* **2003**, *220* (03), 127-130.
2. Flammer, J.; Orgül, S.; Costa, V. P.; Orzalesi, N.; Krieglstein, G. K.; Serra, L. M.; Renard, J.-P.; Stefánsson, E., The impact of ocular blood flow in glaucoma. *Progress in retinal and eye research* **2002**, *21* (4), 359-393.
3. Siesky, B.; Harris, A., The Importance of Ocular Blood Flow in OAG. *Review of Optometry* **2011**, *148* (10), 108-117.